LANGMUIR

pubs.acs.org/Langmuir Article

Dimethyl Sulfoxide-Free and Water-Soluble Fluorescent Probe for Detection of Bovine Serum Albumin Prepared by Ionic Co-assembly of Amphiphiles

Qin Tong, Weichun Wu, Jianghong Hu, Junhao Wang, Ke Li, Bin Dong, and Bo Song*

Cite This: *Langmuir* 2021, 37, 4532−4539

Read Online

ACCESS | Metrics & More | Article Recommendations | Supporting Information

ABSTRACT: Detection of bovine serum albumin (BSA) is an important issue in the sense of medical applications and enzymatic reactions; however, the recently developed fluorescent probes require the involvement of dimethyl sulfoxide (DMSO), which may be detrimental to proteins. In this study, we demonstrated a DMSO-free and water-soluble fluorescent probe prepared by ionic co-assembly of amphiphiles. The cationic amphiphile is a newly designed molecule (denoted by DPP-12) bearing a conjugated diketopyrrolopyrrole (DPP) and two tetraphenylethylene groups. It turns out that the fluorescence emission of DPP-12 depends on the amount of anionic amphiphilic sodium dodecyl benzene sulfonate (SDBS). The fluorescence intensity first increases and then decreases with the concentration of SDBS, and each branch presents a linear relationship. BSA consumes SDBS by the formation of complexes, thus leading to an increase of fluorescence intensity of the mixed solution of DPP-12 and SDBS. Therefore, the mixed solution of DPP-12 and SDBS was applied as a fluorescent probe to detect the low concentration of BSA by back-titration. This fluorescent probe does not require DMSO and has good tolerance to metal ions in blood and good photostability. The limit of detection is as low as 940 nM, almost 3 orders of magnitude lower than the content in organisms.

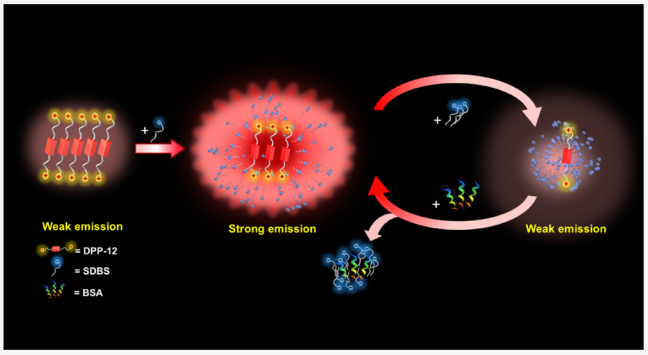

INTRODUCTION

Serum albumin is essential for maintaining the normal nutritional status of the human body and the osmotic pressure of plasma and other colloids.[1−8] The content of serum albumin in blood is an indicator of the nutritional status of an organism.[7,9−12] Too much or too little cycling serum albumin in the blood may be harmful to health. Too much serum albumin may cause heart or kidney diseases,[13−15] and too little serum albumin may cause edema or shock.[16−18] In the sense of medical applications and enzymatic reactions, developing an accurate, fast, and sensitive detection method for serum albumin is highly demanded.[19−23]

Among various serum albumins, bovine serum albumin (BSA) has structural homology with human serum albumin (HSA),[24−26] is readily accessible, and thus being widely studied as a model protein instead of HSA.[27−30] Currently, the developed detection approaches for BSA include Kjeldahl method, biuret method, electrochemical impedance spectroscopy, near-infrared diffuse reflectance spectroscopy, capillary electrophoresis, and light scattering technique.[31−33] Although these approaches show reasonable sensitivity and selectivity, they have several disadvantages, such as the complexity of the procedure, time consumption, and poor reproducibility. Therefore, quick and accurate detection of minimal amounts of BSA, using a biosensing tool with simple design and high precision, is very desirable and presently under active research.[34−36] In this regard, fluorescence spectroscopy with a highly selective and sensitive probe would be potentially applicable and prospective.

Diketopyrrolopyrrole (DPP) derivatives have been widely used as fluorescent probes[37−39] for the detection of BSA[40] because of their ease of synthesis, facility of modification, excellent durability, and attractive optical properties.[41] However, the planar aromatic DPP is water-insoluble,[42] but BSA is water-soluble. The contradictory solubility makes the direct application of DPP in aqueous medium difficult. In order to solve this problem, amphiphiles bearing DPP moieties were designed and synthesized.[43,44] This idea indeed works in aqueous solution, but the unpredictable sedimentation occurring between the amphiphile and BSA causes the inaccuracy of the detection results.[45] Therefore, a certain

Received: January 9, 2021
Revised: March 28, 2021
Published: April 7, 2021

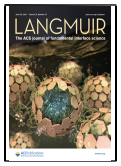

https://doi.org/10.1021/acs.langmuir.1c00072
Langmuir 2021, 37, 4532−4539

amount of dimethyl sulfoxide (DMSO) was usually added into the aqueous solution during the sample preparation.[46] It is known that DMSO may cause precipitation, crystallization, and denaturation of proteins,[47−50] which will inevitably affect the detection results. Using DMSO to depress sedimentation is not an optimal solution.

In this work, we designed and synthesized a cationic bola-amphiphile bearing conjugated DPP and tetraphenylethylene (TPE) moieties in the middle of molecules (denoted by DPP-12). It has been reported that the aromatic conjugates act as fluorescence dyes with an aggregation-induced emission property,[51−54] and thus the resulting compound should have strong fluorescence emission upon self-assembly in aqueous solution. We found that the emission of DPP-12 first increased and then decreased with the addition of an amount of sodium dodecyl benzene sulfonate (SDBS), and both the increase and decrease processes presented a linear correlation in a certain range of concentration of SDBS. BSA and SDBS can form a strong complex, and the reduced SDBS can be reflected by the fluorescence intensity of DPP-12. Therefore, DPP-12 was applied as an indicator of back titration for the detection of BSA. Noteworthily, organic solvents (including DMSO) were not involved all through this study. We believe that this research thus provides a feasible avenue for exploring DMSO-free and water-soluble biosensors for the detection of BSA.

■ MATERIALS AND METHODS

Materials. Sodium *tert*-pentoxide, 1,12-dibromododecane, chloroform-*d* ($CDCl_3$), and DMSO-d_6 were purchased from J&K Chemical Co., Ltd. (Shanghai). Bis(pinacol) diboron and $Pd(PPh_3)_4$ were purchased from Energy Chemical Co., Ltd. Tetrahydrofuran (THF), *N*-methyl pyrrolidone (NMP), methanol, pyridine, Na_2SO_4, NaCl, K_2CO_3, KCl, $CaCl_2$, $MgSO_4$, and $ZnCl_2$ were bought from Sinopharm Chemical Reagent Co., Ltd. (Shanghai). SDBS, diisopropyl succinate, and 1-bromo-1,2,2-triphenylethylene were purchased from TCI Development Co., Ltd. (Shanghai). Ethyl acetate, petroleum ether, and dichloromethane (DCM) were purchased from Yonghua Chemical Technology Co., Ltd. (Jiangsu). 1,4-Dioxane and *tert*-pentoxide were bought from 3A Chemicals Co., Ltd. (Shanghai). $Pd(dppf)Cl_2{\cdot}CH_2Cl_2$, sodium tosylate (ST), and sodium laurate (SL) were purchased from Macklin Biochemical Technology Co., Ltd. (Shanghai). 4-Bromobenzonitrile was purchased from Titan Scientific Co., Ltd. (Shanghai). Newborn calf serum was bought from Beyotime Biotechnology Co., Ltd. Milli-Q water with a resistivity of 18.2 MΩ·cm was produced by Direct-Q 5UV manufactured by Merck Millipore.

Instruments. ^{1}H NMR spectroscopy was performed on Avance III 400 MHz (Bruker, USA) and 600 MHz NMR spectrometers (Agilent Technologies, USA). Mass spectroscopy (MS) of 2,5-bis(12-bromododecyl)-3,6-bis(4-bromophenyl)pyrrolo[3,4-*c*]pyrrole-1,4-(2*H*,5*H*)-dione (compound **b**) was performed on a micro Q-TOF III mass spectrometer (Bruker, USA) using electrospray ionization (ESI) mode, and the mass spectra of 4,4,5,5-tetramethyl-2-(1,2,2-triphenylvinyl)-1,3,2-dioxaborolane (compound **c**), 2,5-bis(12-bromododecyl)-3,6-bis(4-(1,2,2-triphenylvinyl)phenyl)pyrrolo[3,4-*c*]pyrrole-1,4(2*H*,5*H*)-dione (compound **d**), and DPP-12 were obtained on a matrix-assisted laser desorption/ionization time-of-flight MS (MALDI-TOF-MS, Bruker, USA) system. The fluorescence spectra were recorded on FLS980 (Edinburgh Instruments, UK). The ultraviolet−visible (UV−vis) absorption spectra were recorded on Cary 60 (Agilent Technologies, USA). Atomic force microscopy (AFM) images were recorded on a MultiMode 8 microscope (Bruker, USA). Peak force quantitative nanomechanical mapping mode with a ScanAasyst-air probe (nominal spring constant of 0.4 N m^{-1}, frequency 70 kHz, from Bruker) was adopted during the measurement. The samples were cast on a mica substrate and dried in a vacuum. Fourier transform infrared (FTIR) spectra were recorded on Nicolet 6700 produced by Thermo Scientific (USA).

Synthesis and Characterization. *Synthesis of 3,6-Bis(4-bromophenyl)pyrrolo[3,4-c]pyrrole-1,4(2H,5H)-dione (Compound **a**).* 1.73 g of 4-bromobenzonitrile (9.50 mmol) and 2.09 g of sodium *tert*-pentoxide (19 mmol) were added into a 100 mL three-necked flask. Under nitrogen atmosphere, 12 mL of *tert*-amyl alcohol was injected into the flask by a syringe, and then the temperature of the system was raised to 100 °C. After 1 h, 5 mL of *tert*-amyl alcohol with 0.77 mL of diisopropyl succinate (3.80 mmol) was injected, and the mixture was refluxed at 115 °C for 24 h. Then, 5 mL of acetic acid was added, and the mixture reacted at 120 °C for 1 h. The precipitate was obtained by filtration, and the filtered cake was alternatively washed with water (60 °C) and methanol three times. A red solid compound **a** (1.23 g) was obtained with a yield of 75%.

*Synthesis of Compound **b**.* 1.02 g of compound **a** (2.30 mmol) and 1.32 g of potassium *tert*-butoxide (11.20 mmol) were added into a 250 mL three-necked flask. Under nitrogen atmosphere, 40 mL of dry NMP was injected, and the reactant was stirred at 60 °C for 1 h. Then, 4.52 g of 1,12-dibromododecane (13.80 mmol) was added dropwise. The mixture was stirred at 60 °C for 24 h. After being cooled down, the reactant was dissolved in toluene and extracted. The organic layer was collected and dried with anhydrous magnesium sulfate. The product was purified by silica gel column chromatography, using petroleum ether/ethyl acetate (10/1, v/v) as an eluent. The reddish compound **b** (0.62 g) was obtained with a yield of 60%. ^{1}H NMR (400 MHz, $CDCl_3$): δ 7.76−7.63 (m, 8H), 3.78−3.65 (m, 4H), 3.40 (t, J = 6.9 Hz, 4H), 1.85 (p, J = 6.9 Hz, 4H), 1.41 (dd, J = 7.8, 6.1 Hz, 4H), 1.29−1.15 (m, 32H).

*Synthesis of Compound **c**.* 1.04 g of 1-bromo-1,2,2-triphenylethylene (3.10 mmol), 1.18 g of bis(pinacol)diboron (4.65 mmol), and 1.22 g of potassium acetate (12.40 mmol) were added into a 100 mL three-necked flask. Under nitrogen atmosphere, 0.26 g of 1′-bis(diphenylphosphine)ferrocene palladium(II) chloride (0.31 mmol) was added, and then 20 mL of dioxane was injected with a syringe. The mixture reacted at 80 °C for 24 h and then dissolved in DCM and extracted with water. The organic layer was collected and dried with anhydrous magnesium sulfate. The product was purified by silica gel column chromatography, using petroleum ether/DCM (3/1, v/v) as an eluent. A white solid compound **c** (0.65 g) was obtained with a yield of 74%. ^{1}H NMR (400 MHz, $CDCl_3$): δ 7.35 (dq, J = 5.2, 2.7 Hz, 2H), 7.31 (d, J = 6.8 Hz, 3H), 7.14 (t, J = 7.1 Hz, 2H), 7.11−7.07 (m, 4H), 7.07−7.03 (m, 2H), 6.97 (dd, J = 6.5, 2.9 Hz, 2H), 1.13 (s, 12H). ESI-MS (m/z): $[M + 1]^+$ calcd for $C_{26}H_{27}BO_2$, 383.210; found, 383.218.

*Synthesis of Compound **d**.* 0.28 g of compound **b** (0.30 mmol), 0.25 g of compound **c** (0.66 mmol), and 0.02 g of tetrakis(triphenylphosphine)palladium were added to a 100 mL three-necked flask. Under nitrogen protection, 10 mL of THF and 5 mL of potassium carbonate solution (2 M) were added, and the mixture reacted at 66 °C for 24 h. The reactant was extracted with water and DCM, and the organic layer was dried with anhydrous magnesium sulfate. The crude product was purified by silica gel column chromatography, using petroleum ether/DCM (1/2, v/v) as the eluent. An orange solid compound **d** (0.22 g) was obtained with a yield of 57%. ^{1}H NMR (400 MHz, $CDCl_3$): δ 7.57 (d, J = 8.3 Hz, 4H), 7.11−7.00 (m, 34H), 3.67 (t, J = 7.7 Hz, 4H), 3.40 (t, J = 6.8 Hz, 4H), 1.85 (p, J = 7.1 Hz, 4H), 1.12 (s, 36H). MALDI-TOF-MS (m/z): $[M]^+$ calcd for $C_{82}H_{86}Br_2N_2O_2$, 1290.504; found, 1290.706.

Synthesis of DPP-12. 0.12 g of compound **d** (0.1 mmol) was added in 100 mL of pyridine and refluxed at 100 °C for 72 h. Pyridine was removed by Rotavapor, and the solid was washed five times with ethyl ether. A reddish solid DPP-12 (0.11 g) was obtained with a yield of 75%. At 25 °C, 0.094 g DPP-12 can be dissolved in 100 mL of water, and the melting point of DPP-12 is 261 °C. ^{1}H NMR (400 MHz, DMSO-d_6): δ 9.06 (d, J = 6.0 Hz, 4H), 8.58 (t, J = 7.8 Hz, 2H), 8.14 (t, J = 7.0 Hz, 4H), 7.69−6.78 (m, 38H), 4.56 (t, J = 7.5 Hz, 4H), 3.60 (s, 4H), 2.03−1.92 (m, 4H), 1.22 (s, 36H). ^{13}C NMR (100 MHz, DMSO-d_6): δ 161.40, 147.16, 146.21, 145.48, 144.73, 142.79, 142.74, 142.53, 142.01, 139.72, 131.00, 130.69, 130.60, 128.08,

https://doi.org/10.1021/acs.langmuir.1c00072
Langmuir 2021, 37, 4532−4539

Scheme 1. Synthetic Route of DPP-12

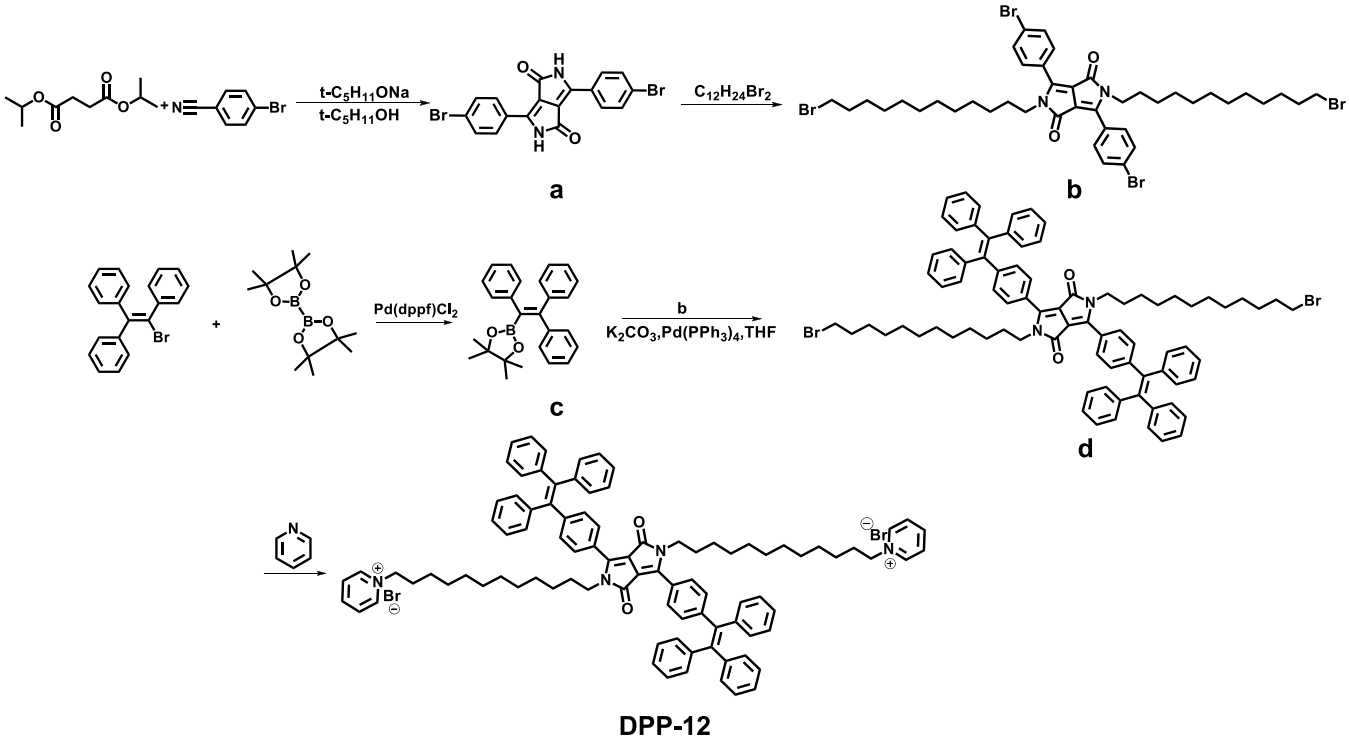

128.03, 127.97, 127.88, 126.86, 125.83, 108.60, 60.73, 30.72, 28.91, 28.86, 28.81, 28.77, 28.41, 28.31, 28.25, 25.92, 25.41. MALDI-TOF-MS (m/z): $[M - Br]^+$ calcd for $C_{92}H_{96}Br_2N_4O_2$, 1369.676; found, 1369.876.

■ RESULTS AND DISCUSSION

The synthetic route of DPP-12 is shown in Scheme 1, and the details of each step of reaction are described in the Materials and Methods section. The characterization, mainly by ^{1}H NMR and MS, of the synthesized products is presented in the Supporting Information. DPP-12 is soluble in water, and the aqueous solution shows an emission peak at around 595 nm (λ_{ex} = 505 nm). The overlap between the absorption and emission bands (Figure S1) is quite small, which means that the self-absorption should be negligible. The plot of fluorescence intensity versus concentration was employed to determine the critical micelle concentration (CMC) of DPP-12.[55,56] As shown in Figure S2, the linear fitting of the data shows an intersection point at 3.3×10^{-5} mol L^{-1}, which is assigned to the CMC of DPP-12. In the following study, a concentration of 1×10^{-4} mol L^{-1} (above CMC) was adopted.

We actually have attempted to use DPP-12 as the fluorescent probe to detect BSA directly but failed because of the formation of precipitate once BSA was added into the aqueous solution of DPP-12 (Figure S3), and the precipitation makes the fluorescent signals NOT reliable. This result is consistent with that reported in the literature.[46] We are pleased to find that the fluorescence emission of DPP-12 responds to SDBS. By increasing the amount of SDBS while keeping the concentration of DPP-12 constant, the fluorescence emission first increases and then decreases until it maintains a constant intensity, as shown in Figure 1. Through linear fitting, we got an intersection point at 1.1×10^{-3} mol L^{-1}. Coincidently, this concentration is very close to the CMC of SDBS (1.2×10^{-3} mol L^{-1}).[57] These results can be reasonably explained by the

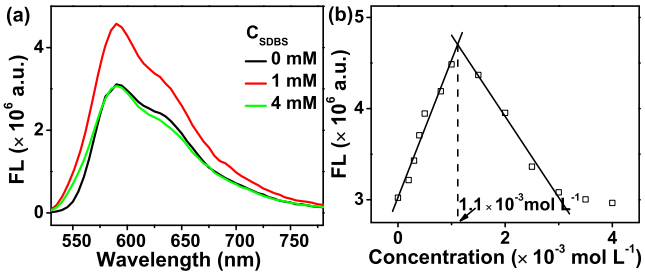

Figure 1. (a) Fluorescence spectra of DPP-12 in the presence of different concentrations of SDBS in aqueous solution. (b) Plot of fluorescence intensity at 595 nm vs C_{SDBS}.

co-assembly of DPP-12 and SDBS through electrostatic interactions. (1) As the concentration of SDBS (denoted by C_{SDBS}) is lower than 1.1×10^{-3} mol L^{-1}, SDBS cannot form micelles alone but co-assemble with DPP-12. As the concentration of DPP-12 adopted here is higher than its CMC, the molecules exist in the solution in the form of micelles instead of individual molecules. Presumably, SDBS molecules were inserted into the micelles of DPP-12, thus forming new assemblies by the complexes of DPP-12 and SDBS. The electrostatic combination will, to some extent, screen the repulsive interaction between the pyridinium groups on DPP-12, and the aromatic conjugates of DPP and TPE that are present inside the micelle have more chances to form closely packed stacking. This could be a reasonable explanation to the enhanced emission of DPP-12. (2) As C_{SDBS} is higher than 1.1×10^{-3} mol L^{-1}, SDBS tends to form micelles. The excess SDBS micelles may encapsulate DPP-12 molecules and thus decompose the initially formed co-assemblies, leading to the decrease of fluorescence emission. When there are enough SDBS micelles to hold all the DPP-12 molecules separately, the fluorescence will not decrease any more, which also explains

https://doi.org/10.1021/acs.langmuir.1c00072
Langmuir 2021, 37, 4532−4539

the constant fluorescence intensity at high concentrations of SDBS. It is worth noting that no observable precipitate appeared in the solution, no matter how much SDBS was added.

To understand the roles played by the alkyl chains and tosylate in the interaction with DPP-12, ST and SL were selected as controls, and the spectral results are shown in Figure S4. ST remarkably reduced the emission of DPP-12. Similar to SDBS, SL first improved and then reduced the emission of DPP-12 by increasing the addition amount. Different with that occurred with SDBS, the changes of fluorescence intensity are fairly small. These results indicate that both the tosylate (showing strong interactions with pyridinium) and the alkyl chains (hydrophobic interactions) are indispensable for the dramatic and parabolic change of fluorescence emission. Fortunately, it is proven later in this study that the complexes formed by SDBS and DPP-12 also showed very good responses to BSA.

We used the absorption spectra to monitor the aggregation state of DPP-12 in the presence of different concentrations of SDBS. As shown in Figure 2, increasing the concentration of

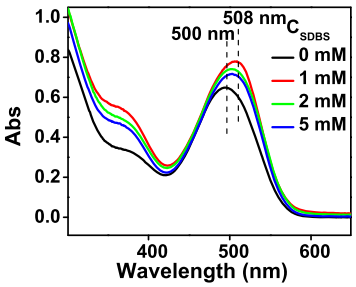

Figure 2. UV−vis spectra of DPP-12 in the presence of different concentrations of SDBS. The concentration of DPP-12 (C_{DPP-12}) is 1 × 10^{-4} mol L^{-1}.

SDBS leads to the shift of the peak from 500 to 508 nm. The bathochromic shift implies that the DPP moieties were packed more closely in the aggregates, which should be ascribed to the balanced electronic repulsion effect between the pyridinium head groups due to the insertion of the negatively charged tosyl groups.[58,59] When C_{SDBS} increased to 5 × 10^{-3} mol L^{-1} (approximately 50 times of that of DPP-12), the absorption peak shifted back. SDBS dominates in the assemblies, and DPP-12, to a greater extent, is segregated by SDBS molecules. This might be a reasonable explanation for the shift of the absorption peak.

The abovementioned assumption that SDBS is inserted into the assemblies of DPP-12 can be proved by the morphological change of the assemblies. As shown by the AFM images in Figure 3, DPP-12 formed irregular nanodiscs with thicknesses of 2−3 nm and diameters in the range of 30−80 nm. As 2 × 10^{-4} mol L^{-1} SDBS was added into the solution of DPP-12 (1 × 10^{-4} mol L^{-1}), the thickness of the nanodiscs kept unchanged, whereas the diameters increased to the range of 300−450 nm. The insertion of SDBS into the assemblies can well explain the size increase of the nanodiscs. As C_{SDBS} increased to 1 × 10^{-3} mol L^{-1}, the nanodiscs shrank to 80−100 nm. Now, the ratio of SDBS to DPP-12 is 10:1, and SDBS became dominating. The excess SDBS forced the nanodiscs to break down into smaller ones. As C_{SDBS} increased to 5 × 10^{-3} mol L^{-1}, 50 times of that of DPP-12, in the vision of AFM image, only particles with size of 30−40 nm were observed. We

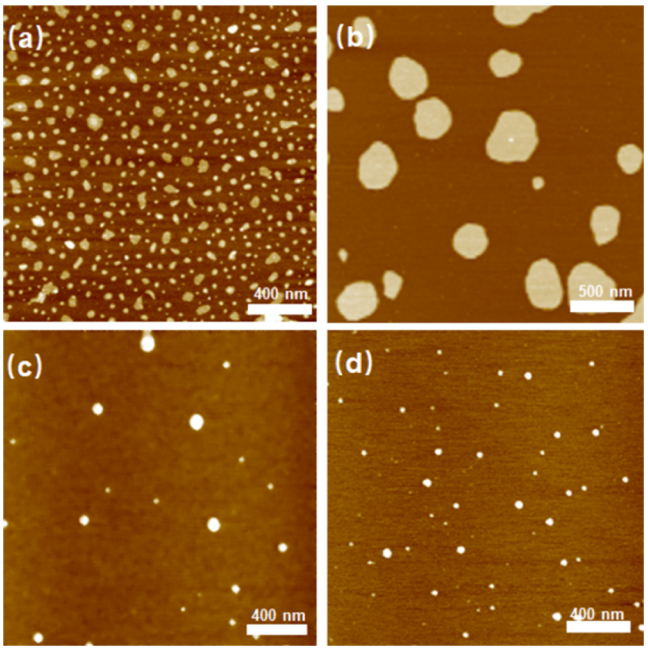

Figure 3. AFM images of the co-assemblies of DPP-12 and SDBS with C_{SDBS} = (a) 0, (b) 2 × 10^{-4}, (c) 1 × 10^{-3}, and (d) 5 × 10^{-3} mol L^{-1}.

believe that these particles should be mainly composed of SDBS molecules with a few DPP-12 molecules in each particle. The morphological change corresponds to the fluorescence decrease as too much SDBS was added to the solution. Based on the above discussion, a schematic illustration of the morphological alternation of the assemblies is summarized in Scheme 2.

Scheme 2. Schematic Illustration of the Morphological and Fluorescence Emission Change of DPP-12 as Being Interacted with SDBS and BSA

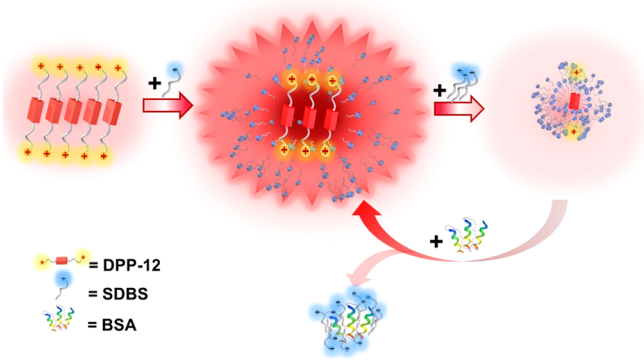

The interaction between DPP-12 and SDBS was qualitatively analyzed by FTIR spectroscopy. As shown in Figure 4a, the peaks at around 1205 and 1133 cm^{-1} are assigned to the antisymmetric and symmetric stretching vibrations of $-SO_3^-$ in SDBS, respectively. When SDBS was added to 2 × 10^{-4} mol L^{-1}, the two peaks shift to 1195 and 1128 cm^{-1}, respectively, which should be attributed to the electrostatic interaction between the sulfonate and pyridinium groups.[60] When the concentration of SDBS increased to 1 × 10^{-3} or 5 × 10^{-3} mol L^{-1}, the signal of the complex was covered by the signal of the sulfonate groups, and hence the vibrational peaks shifted back

https://doi.org/10.1021/acs.langmuir.1c00072
Langmuir 2021, 37, 4532−4539

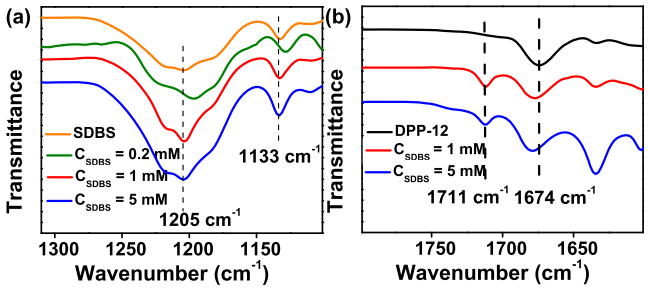

Figure 4. FTIR spectra of (a) SDBS and (b) DPP-12 with different C_{SDBS} values. $C_{DPP\text{-}12} = 1 \times 10^{-4}$ mol L^{-1}.

to 1205 and 1133 cm^{-1}. As shown in Figure 4b, the peaks at 1711 and 1674 cm^{-1} are assigned to the stretching vibration of the carbonyl and stretching vibration of C═C in the DPP moiety. Upon the addition of 2 equiv SDBS, the peak at around 1711 cm^{-1} becomes stronger. This alteration could be explained by the reduced interaction between DPP-12 molecules due to the intercalation of SDBS. The conjugation or delocalization effect produced by the strong π−π stacking interaction suppresses the characteristic peak of the amide carbonyl group. The segregation effect caused by SDBS intercalation will reduce the π−π stacking interaction, so the suppressed amide carbonyl characteristic peak becomes obvious.[61] Because of the reduced π−π stacking interaction, the vibrational peak of C═C shifted to 1678 cm^{-1}. These results are consistent with the change in morphology and can explain the cause of the fluorescence change together.

In the following, the mixed solution of DPP-12 and SDBS was applied to detect BSA, in which the fluorescence intensity of DPP-12 acts as an indicator. Through varying the concentration of SDBS and keeping the concentration of DPP-12 at 1×10^{-4} mol L^{-1} (corresponding spectral results are shown in Figure S5), the optimal concentration of SDBS was 1.7×10^{-3} mol L^{-1}. For convenience of expression, the mixed solution with the above-mentioned optimal concentrations is denoted by BSA-probe. Under these specific conditions, reducing SDBS leads to an increase in the fluorescence intensity of the BSA-probe, which means that the addition of BSA will improve the fluorescence emission of the BSA-probe by reducing the concentration of SDBS. The spectral responses of BSA-probe to different amounts of BSA are presented in Figure 5a. A linear relationship was built between the fluorescence intensity and the concentration of

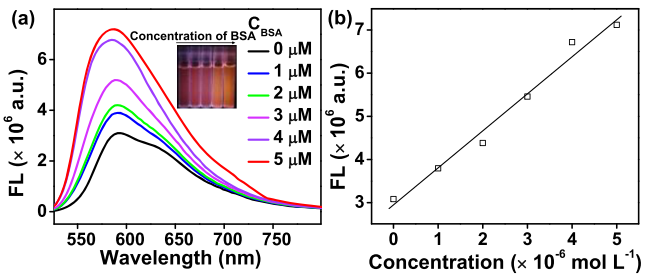

Figure 5. (a) Fluorescence spectra of the mixed solution of DPP-12 and SDBS in the presence of different concentrations of BSA. Inset: photographs of the mixed solution of DPP-12 and SDBS in the presence of different concentrations of BSA. (b) Plot of fluorescence intensity at 595 nm vs BSA. $C_{SDBS} = 1.7 \times 10^{-3}$ mol L^{-1}. $C_{DPP\text{-}12} = 1 \times 10^{-4}$ mol L^{-1}.

BSA (C_{BSA}) in the range of 0−5 μM, as shown in Figure 5b. By linear fitting the data, we can also achieve the limit of detection (LOD) by the equation LOD = $3\sigma/K$, where σ refers to the standard deviation calculated from 10 times the measurement of the fluorescence intensity at 595 nm of the blank sample, and K is the slope of the fitting line.[62] LOD of the mixture probe for BSA is 940 nM, which is far below the limit in organisms (600 μM).[63]

How could BSA improve the fluorescence emission of BSA-probe and even build a good linear relationship? The absorption spectra can be used to answer this question. By carefully controlling the concentration of BSA in the mixed solution, we found that decreasing the concentration of SDBS and increasing the amount of BSA have the same effect, both leading to the peak shift from 500 to 508 nm and both resulting in the enhancement of absorption intensity, as shown in Figures 2 and 6. These results suggest that BSA should have

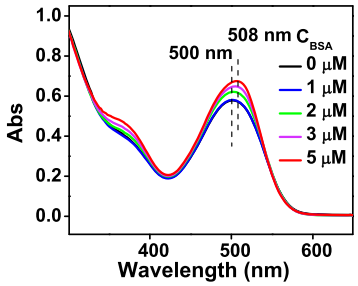

Figure 6. UV−vis spectra of the mixed aqueous solution of DPP-12 and SDBS in the presence of different concentrations of BSA. $C_{DPP\text{-}12} = 1 \times 10^{-4}$ mol L^{-1}.

a specific interaction with SDBS, and the addition of BSA will consume a defined amount of SDBS in the mixed solution, thus leading to an increase in the fluorescence emission.

It has been well documented that the combination of BSA and SDBS will result in an enhanced emission of SDBS residues at around 350 nm.[64] This was verified in our case too. Now, focusing on the fluorescence between 300 and 500 nm, we found that the emission centered at 350 nm indeed increased upon the addition of BSA (Figure S6). Concomitantly, the fluorescence peak at around 330 nm kept unchanged. This is the result of the combination between BSA and SDBS. They are close enough that the energy of tryptophan and tyrosine residues on BSA is able to be transferred to SDBS. These results were consistent with that reported in the literature.[64]

Next, the tolerance of BSA-probe to the metal ions in blood was investigated. Na^+, K^+, Ca^{2+}, Mg^{2+}, and Zn^{2+} are commonly found in blood, and herein, the concentrations of the ions were controlled to the maximum values. As shown in Figure 7a, the above ions have little effect on the fluorescence intensity. Based on the influence of metal ions on the fluorescence intensity, we were able to extrapolate the relative errors to the detection of BSA. The results are listed in Table 1. The maximum relative error was −6.89%, indicating that BSA-probe works nicely even in the presence of these ions.

The photostability of the fluorescent probe was investigated by irradiating the solution by 505 nm light with a power of 2.5 W. As shown in Figure 7b, the fluorescence intensity showed a trivial decrease with the irradiation time. The emission maintained 97% of the initial intensity after the samples were

https://doi.org/10.1021/acs.langmuir.1c00072
Langmuir 2021, 37, 4532−4539

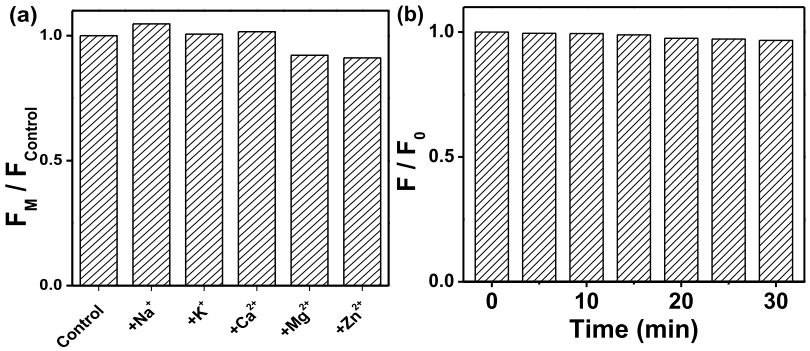

Figure 7. (a) Relative fluorescence intensity at 595 nm in the presence of different metal ions. (b) Photostability of DPP-12. The sample was continuously irradiated by 505 nm light (2.5 W) for 30 min.

Table 1. Effect of Foreign Metal Ions on the Determination of BSA

metal ions	concentration ($\times 10^{-3}$ mol L^{-1})	C_{BSA} founded ($\times 10^{-6}$ mol L^{-1})	relative error (%)
Na^+	145	5.23	4.67
K^+	5.51	5.03	0.61
Ca^{2+}	1.33	5.08	1.58
Mg^{2+}	1.01	4.71	−5.84
Zn^{2+}	0.02	4.66	−6.89

irradiated for 30 min, indicating that the probe owns good photostability under the working conditions.

Finally, BSA-probe was practically applied to detect the BSA content of unknown samples from newborn calf serum. In order to evaluate the detection capability of the probe at different concentrations of BSA, the newborn calf serum was diluted to different concentrations and then added into BSA-probe, where the concentrations of DPP-12 and SDBS were 1×10^{-4} and 1.7×10^{-3} mol L^{-1}, respectively. C_{BSA} in the sample after diluting was obtained by substituting the fluorescence intensity at 595 nm into the original linear fitting equation (in Figures 5b and S7a). For comparison, we also determined the content of BSA by using UV−vis absorption spectra (in Figure S7b). In doing so, pure BSA was employed to build a relationship between the absorption intensity and the concentration of BSA, as shown in Figure S8. Then, the concentrations of BSA in the unknown samples were read from the plot. The results obtained from these two methods are shown in Table 2. First, the two groups of data are comparable

Table 2. Detection of BSA of Unknown Samples

	DPP-12 + SDBS		UV−vis spectra	
sample	C_{BSA} ($\times 10^{-6}$ mol L^{-1})	RSD (%)	C_{BSA} ($\times 10^{-6}$ mol L^{-1})	RSD (%)
1	1.52	1.98	1.59	1.38
2	4.54	1.34	4.62	1.33
3	4.99	1.22	5.11	2.31

for each sample. As shown in Table 2, the BSA concentrations determined by the UV−vis absorption method were relatively higher that those obtained from the fluorescence method. We assume that the discrepancy may be caused by the scattering effect in the absorption spectra, and the scattering has little effect on the fluorescence emission. From this point of view, the fluorescence method may provide more accurate results.

The fluorescent probe formed by the complex of DPP-12 and SDBS is not flawless. Herein, for a fair evaluation, the advantages and disadvantages of the probe are summarized and listed in Table 3.

Table 3. Advantages and Disadvantages of the Fluorescent Probe Formed by the Complex of DPP-12 and SDBS

advantages	disadvantages
DMSO-free	poor selectivity
water-soluble	narrow probing range
good photostability	indirect probing
high accuracy	

■ CONCLUSIONS

In this study, an amphiphile containing a conjugate of one DPP and two TPE groups (i.e., DPP-12) was designed and synthesized. The fluorescence emission of DPP-12 first increases and then decreases with the concentration of added SDBS. In a certain range of concentration, the fluorescence intensity of DPP-12 shows a linear relationship with the amount of SDBS. Another linear relationship is built between the content of BSA and emission of DPP-12 mediated by SDBS, for BSA consumes SDBS in the mixed solution, thus leading to the increase of fluorescence emission of DPP-12. The mixed solution working as a fluorescent probe for the detection of BSA shows very good photostability and high accuracy.

■ ASSOCIATED CONTENT

Supporting Information

The Supporting Information is available free of charge at https://pubs.acs.org/doi/10.1021/acs.langmuir.1c00072.

UV−vis and fluorescence spectra of DPP-12; CMC determination of DPP-12; photographs of the solutions of DPP-12, DPP-12 + BSA, and DPP-12 + SDBS + BSA; fluorescence spectra of DPP-12 in the presence of ST and SL; fluorescence spectra of SDBS and the mixed solution of DPP-12 and SDBS in the presence of BSA; content of BSA determined by UV−vis absorption spectra; ^{1}H NMR spectra of compounds **b**, **c**, **d**, and DPP-12; ^{13}C NMR spectrum of DPP-12; and MS of compounds **b**, **c**, **d**, and DPP-12 (PDF)

https://doi.org/10.1021/acs.langmuir.1c00072
Langmuir 2021, 37, 4532−4539

■ AUTHOR INFORMATION

Corresponding Author

Bo Song − *College of Chemistry, Chemical Engineering and Materials Science, Soochow University, Suzhou 215123, P. R. China*; orcid.org/0000-0002-7546-9482; Email: songbo@suda.edu.cn

Authors

Qin Tong − *College of Chemistry, Chemical Engineering and Materials Science, Soochow University, Suzhou 215123, P. R. China*

Weichun Wu − *College of Chemistry, Chemical Engineering and Materials Science, Soochow University, Suzhou 215123, P. R. China*

Jianghong Hu − *College of Chemistry, Chemical Engineering and Materials Science, Soochow University, Suzhou 215123, P. R. China*

Junhao Wang − *College of Chemistry, Chemical Engineering and Materials Science, Soochow University, Suzhou 215123, P. R. China*

Ke Li − *College of Chemistry, Chemical Engineering and Materials Science, Soochow University, Suzhou 215123, P. R. China*

Bin Dong − *College of Chemistry, Chemical Engineering and Materials Science, Soochow University, Suzhou 215123, P. R. China*; orcid.org/0000-0001-5681-372X

Complete contact information is available at: https://pubs.acs.org/10.1021/acs.langmuir.1c00072

Notes

The authors declare no competing financial interest.

■ ACKNOWLEDGMENTS

The authors are thankful to the National Natural Science Foundation of China (21674075), the Natural Science Foundation of Jiangsu Province (BK20161211), the Key University Science Research Project of Jiangsu Province (17KJA150007), Suzhou Key Laboratory of Macromolecular Design and Precision Synthesis, Jiangsu Key Laboratory of Advanced Functional Polymer Design and Application, a project funded by the Priority Academic Program Development of Jiangsu Higher Education Institutions, and State and Local Joint Engineering Laboratory for Novel Functional Polymeric Materials.

■ REFERENCES

(1) Olson, R. E.; Christ, D. D. Plasma protein binding of drugs. *Annual Reports in Medicinal Chemistry*; Academic Press: Orlando, 1996; Vol. *31*, pp 327−336.

(2) Nicholson, J. P.; Wolmarans, M. R.; Park, G. R. The role of albumin in critical illness. *Br. J. Anaesth.* **2000**, *85*, 599−610.

(3) Wen, J.; Geng, Z.; Yin, Y.; Wang, Z. A versatile water soluble fluorescent probe for ratiometric sensing of Hg^{2+} and bovine serum albumin. *Dalton Trans.* **2011**, *40*, 9737−9745.

(4) Peters, T., Jr. Serum albumin. *Advances in Protein Chemistry*; Academic Press: San Diego, 1985; Vol. *37*, pp 161−245.

(5) He, X. M.; Carter, D. C. Atomic structure and chemistry of human serum albumin. *Nature* **1992**, *358*, 209−215.

(6) Corti, M. C.; Guralnik, J. M.; Salive, M. E.; Sorkin, J. D. Serum-albumin level and physical-disability as predictors of mortality in older persons. *JAMA, J. Am. Med. Assoc.* **1994**, *272*, 1036−1042.

(7) Don, B. R.; Kaysen, G. Poor nutritional status and inflammation: serum albumin: relationship to inflammation and nutrition. *Semin. Dial.* **2004**, *17*, 432−437.

(8) Mafina, M.-K.; Hing, K. A.; Sullivan, A. C. Development of novel fluorescent probes for the analysis of protein interactions under physiological conditions with medical devices. *Langmuir* **2013**, *29*, 1420−1426.

(9) Bai, H.; Qian, J.; Tian, H.; Pan, W.; Zhang, L.; Zhang, W. Fluorescent polarity probes for identifying bovine serum albumin: Amplification effect of para-substituted benzene. *Dyes Pigm.* **2014**, *103*, 1−8.

(10) Forse, R. A.; Shizgal, H. M. Serum albumin and nutritional status. *J. Parenter. Enteral Nutr.* **1980**, *4*, 450−454.

(11) Gariballa, S. E.; Parker, S. G.; Taub, N.; Castleden, C. M. Influence of nutritional status on clinical outcome after acute stroke. *Am. J. Clin. Nutr.* **1998**, *68*, 275−281.

(12) Shenkin, A. Serum prealbumin: is it a marker of nutritional status or of risk of malnutrition? *Clin. Chem.* **2006**, *52*, 2177−2179.

(13) Curry, S. Beyond expansion: structural studies on the transport roles of human serum albumin. *Vox Sang.* **2002**, *83*, 315−319.

(14) Gibbs, J.; Cull, W.; Henderson, W.; Daley, J.; Hur, K.; Khuri, S. F. Preoperative serum albumin level as a predictor of operative mortality and morbidity—Results from the national VA surgical risk study. *Arch. Surg.* **1999**, *134*, 36−42.

(15) Dziedzic, T.; Slowik, A.; Szczudlik, A. Serum albumin level as a predictor of ischemic stroke outcome. *Stroke* **2004**, *35*, e156−e158.

(16) Hu, Y.-J.; Liu, Y.; Shen, X.-S.; Fang, X.-Y.; Qu, S.-S. Studies on the interaction between 1-hexylcarbamoyl-5-fluorouracil and bovine serum albumin. *J. Mol. Struct.* **2005**, *738*, 143−147.

(17) Herrmann, F. R.; Safran, C.; Levkoff, S. E.; Minaker, K. L. Serum-albumin level on admission as a predictor of death, length of stay, and readmission. *Arch. Intern. Med.* **1992**, *152*, 125−130.

(18) Fasanmade, A. A.; Adedokun, O. J.; Olson, A.; Strauss, R.; Davis, H. M. Serum albumin concentration: a predictive factor of infliximab pharmacokinetics and clinical response in patients with ulcerative colitis. *Int. J. Clin. Pharmacol. Ther.* **2010**, *48*, 297−308.

(19) Vitzthum, F.; Geiger, G.; Bisswanger, H.; Brunner, H.; Bernhagen, J. A quantitative fluorescence-based microplate assay for the determination of double-stranded DNA using SYBR Green I and a standard ultraviolet transilluminator gel imaging system. *Anal. Biochem.* **1999**, *276*, 59−64.

(20) Lu, H.; Wang, K.; Liu, B.; Wang, M.; Huang, M.; Zhang, Y.; Yang, J. Systematic oligoaniline-based derivatives: ACQ−AIE conversion with a tunable insertion effect and quantitative fluorescence "turn-on" detection of BSA. *Mater. Chem. Front.* **2019**, *3*, 331−338.

(21) Liu, C.; Yang, W.; Gao, Q.; Du, J.; Luo, H.; Liu, Y.; Yang, C. Differential recognition and quantification of HSA and BSA based on two red-NIR fluorescent probes. *J. Lumin.* **2018**, *197*, 193−199.

(22) Liu, J.-M.; Lin, L.-p.; Wang, X.-X.; Lin, S.-Q.; Cai, W.-L.; Zhang, L.-H.; Zheng, Z.-Y. Highly selective and sensitive detection of Cu^{2+} with lysine enhancing bovine serum albumin modified-carbon dots fluorescent probe. *Analyst* **2012**, *137*, 2637−2642.

(23) Yuan, G.; Kienzle, P. A.; Satija, S. K. Salting up and salting down of bovine serum albumin layers at the air-water interface. *Langmuir* **2020**, *36*, 15240−15246.

(24) Gelamo, E. L.; Silva, C. H. T. P.; Imasato, H.; Tabak, M. Interaction of bovine (BSA) and human (HSA) serum albumins with ionic surfactants: spectroscopy and modelling. *Biochim. Biophys. Acta* **2002**, *1594*, 84−99.

(25) Sułkowska, A. Interaction of drugs with bovine and human serum albumin. *J. Mol. Struct.* **2002**, *614*, 227−232.

(26) Kawamura, R.; Mishima, M.; Ryu, S.; Arai, Y.; Okose, M.; Silberberg, Y. R.; Rao, S. R.; Nakamura, C. Controlled cell adhesion using a biocompatible anchor for membrane-conjugated bovine serum albumin/bovine serum albumin mixed layer. *Langmuir* **2013**, *29*, 6429−6433.

(27) Lin, S.; Liu, S.; Ye, F.; Xu, L.; Zeng, W.; Wang, L.; Li, L.; Beuerman, R.; Cao, D. Sensitive detection of DNA by hyperbranched diketopyrrolopyrrole-based conjugated polyelectrolytes. *Sens. Actuators, B* **2013**, *182*, 176−183.

(28) Akhuli, A.; Chakraborty, D.; Agrawal, A. K.; Sarkar, M. Probing the interaction of bovine serum albumin with copper nanoclusters: realization of binding pathway different from protein corona. *Langmuir* **2021**, *37*, 1823−1837.
(29) Fries, M. R.; Conzelmann, N. F.; Günter, L.; Matsarskaia, O.; Skoda, M. W. A.; Jacobs, R. M. J.; Zhang, F.; Schreiber, F. Bulk phase behavior vs interface adsorption: specific multivalent cation and anion effects on BSA interactions. *Langmuir* **2021**, *37*, 139−150.
(30) Ma, G. J.; Ferhan, A. R.; Jackman, J. A.; Cho, N.-J. Elucidating how different amphipathic stabilizers affect BSA protein conformational properties and adsorption behavior. *Langmuir* **2020**, *36*, 10606−10614.
(31) Comper, W. D.; Osicka, T. M. Detection of urinary albumin. *Adv. Chronic Kidney Dis.* **2005**, *12*, 170−176.
(32) Wang, Z.; Hoy, W. E.; Nicol, J. L.; Wang, Z.; Su, Q.; Atkins, R. C.; Polkinghorne, K. R. Predictive value of nephelometric and high-performance liquid chromatography assays of urine albumin for mortality in a high-risk Aboriginal population. *Am. J. Kidney Dis.* **2008**, *52*, 672−682.
(33) Miller, W. G.; Bruns, D. E.; Hortin, G. L.; Sandberg, S.; Aakre, K. M.; McQueen, M. J.; Itoh, Y.; Lieske, J. C.; Seccombe, D. W.; Jones, G.; Bunk, D. M.; Curhan, G. C.; Narva, A. S. Current issues in measurement and reporting of urinary albumin excretion. *Clin. Chem.* **2009**, *55*, 24−38.
(34) Jung, H. S.; Chen, X.; Kim, J. S.; Yoon, J. Recent progress in luminescent and colorimetric chemosensors for detection of thiols. *Chem. Soc. Rev.* **2013**, *42*, 6019−6031.
(35) Yin, J.; Kwon, Y.; Kim, D.; Lee, D.; Kim, G.; Hu, Y.; Ryu, J.-H.; Yoon, J. Preparation of a cyanine-based fluorescent probe for highly selective detection of glutathione and its use in living cells and tissues of mice. *Nat. Protoc.* **2015**, *10*, 1742−1754.
(36) Guo, Z.; Park, S.; Yoon, J.; Shin, I. Recent progress in the development of near-infrared fluorescent probes for bioimaging applications. *Chem. Soc. Rev.* **2014**, *43*, 16−29.
(37) Kaur, M.; Choi, D. H. Diketopyrrolopyrrole: brilliant red pigment dye-based fluorescent probes and their applications. *Chem. Soc. Rev.* **2015**, *44*, 58−77.
(38) Li, W.; Wang, L.; Tang, H.; Cao, D. Diketopyrrolopyrrole-based fluorescent probes for detection and bioimaging: Current progresses and perspectives. *Dyes Pigm.* **2019**, *162*, 934−950.
(39) Gao, Y.; Feng, G.; Jiang, T.; Goh, C.; Ng, L.; Liu, B.; Li, B.; Yang, L.; Hua, J.; Tian, H. Biocompatible nanoparticles based on diketo-pyrrolo-pyrrole (DPP) with aggregation-induced Red/NIR emission for in vivo two-photon fluorescence imaging. *Adv. Funct. Mater.* **2015**, *25*, 2857−2866.
(40) Heyer, E.; Lory, P.; Leprince, J.; Moreau, M.; Romieu, A.; Guardigli, M.; Roda, A.; Ziessel, R. Highly fluorescent and water-soluble diketopyrrolopyrrole dyes for bioconjugation. *Angew. Chem., Int. Ed.* **2015**, *54*, 2995−2999.
(41) Hao, Z.; Iqbal, A. Some aspects of organic pigments. *Chem. Soc. Rev.* **1997**, *26*, 203−213.
(42) Iqbal, A.; Jost, M.; Kirchmayr, R.; Pfenninger, J.; Rochat, A.; Wallquist, O. The synthesis and properties of 1, 4-diketo-pyrrolo[3,4-C]pyrroles. *Bull. Soc. Chim. Belg.* **1988**, *97*, 615−644.
(43) Hang, Y.; Yang, L.; Qu, Y.; Hua, J. A new diketopyrrolopyrrole-based near-infrared (NIR) fluorescent biosensor for BSA detection and AIE-assisted bioimaging. *Tetrahedron Lett.* **2014**, *55*, 6998−7001.
(44) Wang, L.; Yang, L.; Cao, D. Probes based on diketopyrrolo-pyrrole and anthracenone conjugates with aggregation-induced emission characteristics for pH and BSA sensing. *Sens. Actuators, B* **2015**, *221*, 155−166.
(45) Sharma, V.; Yañez, O.; Alegría-Arcos, M.; Kumar, A.; Thakur, R. C.; Cantero-López, P. A physicochemical and conformational study of co-solvent effect on the molecular interactions between similarly charged protein surfactant (BSA-SDBS) system. *J. Chem. Thermodyn.* **2020**, *142*, 106022.
(46) Sharma, V.; Cantero-López, P.; Yañez-Osses, O.; Rojas-Fuentes, C.; Kumar, A. Influence of BSA on micelle formation of SDBS and CPC: An experimental−theoretical approach of its binding properties. *J. Mol. Liq.* **2018**, *271*, 443−451.
(47) Arakawa, T.; Kita, Y.; Timasheff, S. N. Protein precipitation and denaturation by dimethyl sulfoxide. *Biophys. Chem.* **2007**, *131*, 62−70.
(48) Ramesh, P.; Shalini, B.; Fadnavis, N. W. Knoevenagel condensation of diethylmalonate with aldehydes catalyzed by immobilized bovine serum albumin (BSA). *RSC Adv.* **2014**, *4*, 7368−7373.
(49) Tjernberg, A.; Markova, N.; Griffiths, W. J.; Hallén, D. DMSO-related effects in protein characterization. *J. Biomol. Screening* **2006**, *11*, 131−137.
(50) Kundu, S.; Malik, S.; Ghosh, M.; Nandi, S.; Pyne, A.; Debnath, A.; Sarkar, N. A comparative study on DMSO-induced modulation of the structural and dynamical properties of model bilayer membranes. *Langmuir* **2021**, *37*, 2065−2078.
(51) Fang, W.; Zhang, G.; Chen, J.; Kong, L.; Yang, L.; Bi, H.; Yang, J. An AIE active probe for specific sensing of Hg^{2+} based on linear conjugated bis-Schiff base. *Sens. Actuators, B* **2016**, *229*, 338−346.
(52) Zhou, S.; Zhao, H.; Feng, R.; Ding, L.; Li, Z.; Deng, C.; He, Q.; Liu, Y.; Song, B.; Li, Y. Application of amphiphilic fluorophore-derived nanoparticles to provide contrast to human embryonic stem cells without affecting their pluripotency and to monitor their differentiation into neuron-like cells. *Acta Biomater.* **2018**, *78*, 274−284.
(53) Su, Y.; Lv, C.; Zhang, Y.; Liu, S.; Xie, Z.; Zheng, M. Fluorescent nanoparticles with ultralow chromophore loading for long-term tumor-targeted imaging. *Acta Biomater.* **2020**, *111*, 398−405.
(54) Shi, J.; Wang, M.; Sun, Z.; Liu, Y.; Guo, J.; Mao, H.; Yan, F. Aggregation-induced emission-based ionic liquids for bacterial killing, imaging, cell labeling, and bacterial detection in blood cells. *Acta Biomater.* **2019**, *97*, 247−259.
(55) Goon, P.; Manohar, C.; Kumar, V. V. Determination of critical micelle concentration of anionic surfactants: comparison of internal and external fluorescent probes. *J. Colloid Interface Sci.* **1997**, *189*, 177−180.
(56) Domínguez, A.; Fernández, A.; González, N.; Iglesias, E.; Montenegro, L. Determination of critical micelle concentration of some surfactants by three techniques. *J. Chem. Educ.* **1997**, *74*, 1227.
(57) Rosen, M. J.; Kunjappu, J. T. *Surfactants and Interfacial Phenomena*, 4th ed.; Wiley: Hoboken, NJ, 2012; pp 123−201.
(58) Song, B.; Wang, Z.; Chen, S.; Zhang, X.; Fu, Y.; Smet, M.; Dehaen, W. The introduction of $\pi-\pi$ stacking moieties for fabricating stable micellar structure: formation and dynamics of disklike micelles. *Angew. Chem., Int. Ed.* **2005**, *44*, 4731−4735.
(59) Wu, G.; Thomas, J.; Smet, M.; Wang, Z.; Zhang, X. Controlling the self-assembly of cationic bolaamphiphiles: hydrotropic counter-anions determine aggregated structures. *Chem. Sci.* **2014**, *5*, 3267−3274.
(60) Zhang, L.; Zhou, S.; Min, S.; Yu, X.; Hou, G.; Tong, Q.; Dong, B.; Zhu, H.; Song, B. Water-soluble near-infrared fluorescent probes enhanced by ionic co-assembly of a four-armed amphiphile with SDBS: Toward application in cell imaging. *Dyes Pigm.* **2020**, *181*, 108541.
(61) Xing, Y.; Li, D.; Dong, B.; Wang, X.; Wu, C.; Ding, L.; Zhou, S.; Fan, J.; Song, B. Water-soluble and highly emissive near-infrared nano-probes by co-assembly of ionic amphiphiles: towards application in cell imaging. *New J. Chem.* **2019**, *43*, 8059−8066.
(62) Analytical Methods Committee. Recommendations for the definition, estimation and use of the detection limit. *Analyst* **1987**, *112*, 199−204.
(63) Peters, T., Jr. *All About Albumin: Biochemistry, Genetics, and Medical Applications*, 1st ed.; Academic Press: San Diego, CA, 1995; pp 9−75.
(64) Sun, C. X.; Wu, X.; Zhou, H. P.; Wang, F.; Ding, H. H.; Zhao, L. L.; Yang, J. H. Ag island film-enhanced rare earth co-luminescence effect of Tb-Gd-protein-sodium dodecyl benzene sulfonate system and sensitive detection of protein. *Talanta* **2008**, *76*, 1047−1052.

https://doi.org/10.1021/acs.langmuir.1c00072
Langmuir 2021, 37, 4532−4539